

Thickness-dependent exciton relaxation dynamics of few-layer rhenium diselenide

Chang-Fu Huo(霍唱福), Tiantian Yun(云田田), Xiao-Qing Yan(鄢小卿), Zewen Liu(刘泽文), Xin Zhao(赵欣), Wenxiong Xu(许文雄), Qiannan Cui(崔乾楠), Zhi-Bo Liu(刘智波), and Jian-Guo Tian(田建国)

Citation: Chin. Phys. B, 2023, 32 (**6**): 067203. DOI: 10.1088/1674-1056/acc1d3
Journal homepage: http://cpb.iphy.ac.cn; http://iopscience.iop.org/cpb

What follows is a list of articles you may be interested in

Modulation of carrier lifetime in MoS_2 monolayer by uniaxial strain

Hao Hong(洪浩), Yang Cheng(程阳), Chunchun Wu(吴春春), Chen Huang(黄琛), Can Liu(刘灿), Wentao Yu(于文韬), Xu Zhou(周旭), Chaojie Ma(马超杰), Jinhuan Wang(王金焕), Zhihong Zhang(张智宏), Yun Zhao(赵芸), Jie Xiong(熊杰), Kaihui Liu(刘开辉)

Chin. Phys. B, 2020, 29 (**7**): 077201. DOI: 10.1088/1674-1056/ab99ba

Effect of strain on exciton dynamics in monolayer WS_2

Lu Zhang(张璐), Da-Wei He(何大伟), Jia-Qi He(何家琪), Yang Fu(付洋), Yong-Sheng Wang(王永生)

Chin. Phys. B, 2019, 28 (**8**): 087201. DOI: 10.1088/1674-1056/28/8/087201

Spin depolarization dynamics of WSe_2 bilayer

Binghui Niu(牛秉慧), Jialiang Ye(叶加良), Ting Li(李婷), Ying Li(李莹), Xinhui Zhang(张新惠)

Chin. Phys. B, 2018, 27 (**5**): 057202. DOI: 10.1088/1674-1056/27/5/057202

Ultrafast interlayer photocarrier transfer in graphene-$MoSe_2$ van der Waals heterostructure

Xin-Wu Zhang(张心悟), Da-Wei He(何大伟), Jia-Qi He(何佳琪), Si-Qi Zhao(赵思淇), Sheng-Cai Hao(郝生财), Yong-Sheng Wang(王永生), Li-Xin Yi(衣立新)

Chin. Phys. B, 2017, 26 (**9**): 097202. DOI: 10.1088/1674-1056/26/9/097202

Electric field-induced hole injection-enhanced photoluminescence in a N,N'-bis(3-methylphenyl)-N,N'-bis(phenyl)-benzidine-based emitter

Xu-Xie Hui-Na (许谢慧娜), Li Wen-Bin (李文彬), Peng Huan (彭欢), He Yun (何鋆), Yu Hao-Miao (于浩淼), Hou Xiao-Yuan (侯晓远)

Chin. Phys. B, 2014, 23 (**4**): 047202. DOI: 10.1088/1674-1056/23/4/047202

Thickness-dependent exciton relaxation dynamics of few-layer rhenium diselenide

Chang-Fu Huo(霍唱福)[1,†], Tiantian Yun(云田田)[1,†], Xiao-Qing Yan(鄢小卿)[1,‡], Zewen Liu(刘泽文)[1], Xin Zhao(赵欣)[2], Wenxiong Xu(许文雄)[3], Qiannan Cui(崔乾楠)[3], Zhi-Bo Liu(刘智波)[1,4,§], and Jian-Guo Tian(田建国)[1]

[1] *Key Laboratory of Weak-Light Nonlinear Photonics, Ministry of Education, School of Physics, Nankai University, Tianjin* 300071, *China*
[2] *School of Physical Science and Technology, Tiangong University, Tianjin* 300387, *China*
[3] *State Key Laboratory of Bioelectronics, School of Biological Science and Medical Engineering, Southeast University, Nanjing* 210096, *China*
[4] *Collaborative Innovation Center of Extreme Optics, Shanxi University, Taiyuan* 030006, *China*

(Received 16 December 2022; revised manuscript received 16 February 2023; accepted manuscript online 7 March 2023)

Rhenium diselenide ($ReSe_2$) has gathered much attention due to its low symmetry of lattice structure, which makes it possess in-plane anisotropic optical, electrical as well as excitonic properties and further enables $ReSe_2$ have an important application in optoelectronic devices. Here, we report the thickness-dependent exciton relaxation dynamics of mechanically exfoliated few-layer $ReSe_2$ flakes by using time-resolved pump–probe transient transmission spectroscopies. The results reveal two thickness-dependent relaxation processes of the excitons. The fast one correlates with the exciton formation (*i.e.*, the conversion of hot carriers to excitons), while the slow one is attributed to the exciton recombination dominated by defect-assisted exciton trapping besides photon emission channel. The decrease of scattering probability caused by defects leads to the increase of fast lifetime with thickness, and the increase of slow lifetime with thickness is related to the trap-mediated exciton depopulation induced by surface defects. Polarization-dependent transient spectroscopy indicates the isotropic exciton dynamics in the two-dimensional (2D) plane. These results are insightful for better understanding of excitonic dynamics of $ReSe_2$ materials and its application in future optoelectronic and electronic devices.

Keywords: rhenium diselenide, pump–probe spectroscopy, carrier dynamics, exciton

PACS: 72.80.Ga, 78.20.–e, 78.47.D–, 78.47.jb **DOI:** 10.1088/1674-1056/acc1d3

1. Introduction

$ReSe_2$ is an emerging member in the transition metal dichalcogenides (TMDs) family.[1] Unlike other 2H-type TMDs members,[2–5] the metal Re atoms form a one-dimensional chain in the plane so that $ReSe_2$ contains metal–metal and metal–sulfur bonds (Fig. 1(a)).[6–9] As a result, it exhibits a distorted 1*T* phase with triclinic symmetry of octahedral crystal structure which results in strong in-plane anisotropy of physical properties,[1,10,11] such as anisotropic optical absorbance[12] and photoresponsivity,[13] as well as orientation-dependent bandgap.[6] Owing to its unique in-plane anisotropic properties, atomically thin $ReSe_2$ films have been applied in polarization-sensitive photoelectric device with a high responsivity,[13] adding an additional degree of freedom to the design and fabrication of devices.

Moreover, previous theoretical calculation and optical absorption measurements have explored the variation of energy bandgap and physical properties of $ReSe_2$ with thickness.[7,14,15] The results of Zhao *et al.* indicated the bandgap in $ReSe_2$ varies with thickness from 1.26 eV (bulk) to 1.32 eV (monolayer) as $ReSe_2$ is thinned.[16] And, optical absorption measurements indicate that optical bandgap of bulk $ReSe_2$ single crystal is 1.19 eV at room temperature.[17] However, from photoluminescence (PL) measurements, Jariwala *et al.* reported that the bandgap of $ReSe_2$ is weakly layer-dependent and increases from 1.29 eV (thick flakes) to 1.31 eV (thin layers).[18] Clearly, the bandgap of $ReSe_2$ has not been exactly determined.

Since the electronic bandgaps and physical properties of $ReSe_2$ vary slightly with thickness, thus it seems that we do not need to use extremely thin $ReSe_2$ layers like other 2D optoelectronic devices when fabricating $ReSe_2$ optoelectronic devices. In other words, the optoelectronic devices with different-thicknesses of $ReSe_2$ exhibit similar properties. If so, it will greatly reduce the difficulty of device fabrication, and further expand the application of $ReSe_2$ in optoelectronic devices. The performance of optoelectronic devices depends on the optical response process and the carrier dynamic properties of the materials used. Therefore, a thorough understanding of these properties is essential. To reveal whether $ReSe_2$ optoelectronic devices have strong dependence on $ReSe_2$ thickness, we could first explore how the carrier dynamics varies with $ReSe_2$ thickness. Up to now, the relaxation of photoexcited carriers in monolayer $ReSe_2$ or bulk $ReSe_2$ has been studied by several groups.[19–23] However, these reports cannot reveal the dependence of carrier dynamics processes on

[†]These authors contributed equally to this work.
[‡]Corresponding author. E-mail: yanxq01@nankai.edu.cn
[§]Corresponding author. E-mail: liuzb@nankai.edu.cn

© 2023 Chinese Physical Society and IOP Publishing Ltd

the $ReSe_2$ thickness since the results of available thickness are very limited and the samples they measured were prepared by direct chemical synthesis methods, which could alter the sample quality and further the carrier dynamics process. In addition, it is difficult to obtain identical quality for adjacent layers in multilayer $ReSe_2$ films produced by direct chemical synthesis methods, limiting our access to the intrinsic thickness-dependence of carrier relaxation in chemically synthesized $ReSe_2$. To explore the variation of carrier relaxation with $ReSe_2$ thickness, it is necessary to study the carrier dynamics in $ReSe_2$ sample prepared via mechanical exfoliation, which could greatly reduce the quality difference for adjacent layers.

In this paper, the time-resolved pump–probe transient transmission spectroscopy is employed to study the exciton dynamics of mechanically exfoliated $ReSe_2$ flakes with thickness varying from 3.6 nm to 49.0 nm. Negative transient differential transmission (ΔT) signal originating from exciton absorption is observed, and two exciton relaxation processes with different lifetimes are extracted from its time-evolution curves. Lifetimes of both processes monotonically increase as thickness increases. The independence of the two relaxation lifetimes on pump power excludes the contributions of exciton–exciton annihilation (EEA) to exciton relaxation. Fast recovery times and slow relaxation times are attributed to the exciton formation and exciton recombination, respectively. Trap-mediated exciton depopulation caused by defects dominates the exciton recombination process besides the photon emission pathway. The results of polarization-resolved ΔT measurements indicate the isotropic exciton relaxation processes in the anisotropic 2D plane. This research makes an important step in understanding and manipulating the properties of $ReSe_2$ via thickness, which will promote its application in the nano-optoelectronic devices.

2. Sample preparation and characterization

Few-layer $ReSe_2$ flakes with different thicknesses are mechanically exfoliated onto a fused quartz from bulk crystal. Figure 1(b) depicts the optical microscopic image of a representative sample on substrate. Transparent substrate makes the uncovered area be black. We use atomic force microscopy (AFM) to determine the height and profile of these few-layer $ReSe_2$ flakes, and the AFM morphologies indicate these flakes have good continuity and homogeneity. The AFM morphology of flake with thickness of $\sim$ 18.6 nm is shown in Fig. 1(c). The AFM morphologies of other samples are depicted in Fig. S1 (supporting information).

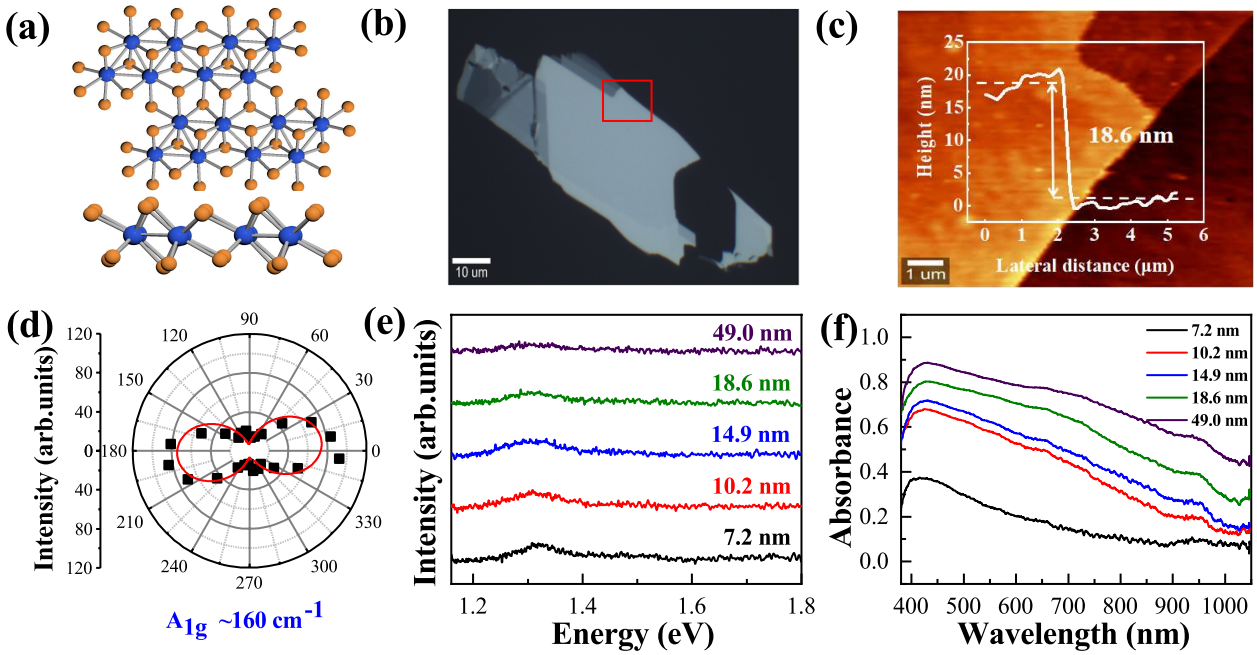


Fig. 1. Crystal structure and characterization of $ReSe_2$ flake. (a) Top and side views of the structure of single $ReSe_2$ layer. (b) Optical microscopic image of mechanically exfoliated few-layer $ReSe_2$ flake. The red rectangle represents the measured area. (c) AFM image of $ReSe_2$ flake shown in panel (b), inset: the corresponding height profile. (d) Polar plots of angle-resolved polarized Raman scattering intensities of the A_{1g} mode. (e) PL spectrum with thickness. (f) Absorption spectra of $ReSe_2$ with different thicknesses.

Polarization dependent Raman spectra measurements, under 532-nm laser excitation, were performed to assess the orientation of b axis in the 2D plane. The polarizations of excitation and scattered light are parallel configuration. The representative polarized-Raman spectra are shown in Fig. S2, and two typical Raman modes at $\sim$ 125 (E_{2g}) and $\sim$ 160 cm^{-1} (A_{1g}) are observed. Figure 1(d) summaries the dependence of the peak intensity of A_{1g} mode on the polarization orientation (the blue arrow shown in Fig. S2) angle θ, which is defined as the angle between the polarized direction of excitation light

and b axis. Clearly, the peak intensity changes with angle θ with an oscillating periodicity of 180°. Previous reports reveal that the strongest scattering of A_{1g} mode occurs nearby the crystal axis of Re chain (*i.e.*, b axis),[7,24] so the 0° corresponds to the direction of the Re chains of $ReSe_2$. The red line through the experimental data is a cosine function fit.

PL measurements were performed to deduce the variation of optical bandgap with thickness. Figure 1(e) shows the PL spectrum of representative $ReSe_2$ samples with different thicknesses, the PL emission is extremely weak due to the intrinsic indirect-bandgap nature of $ReSe_2$. Because carrier recombination in indirect bandgap semiconductor needs the assistance from phonons to keep conservation of momentum, as a result, the radiation probability is greatly reduced. And, the PL spectra show that the exciton peak locates around 1.31 eV, which is in accordance with the results of Jariwala *et al.*[18] Moreover, the PL spectrum of $ReSe_2$ with 3.6-nm thickness indicates the exciton peak at the $\sim$ 1.33 eV (Fig. S3). Remarkably, the exciton peak shifts slightly from $\sim$ 1.33 eV to $\sim$ 1.29 eV as the thickness of $ReSe_2$ increases, implying that the bandgap of $ReSe_2$ is nearly independent on the thickness and weak interlayer coupling in the $ReSe_2$ samples. The PL intensity decreases as $ReSe_2$ thickness increases, which is in accordance with previous reports.[18,25–27] The decrease of PL emission intensity with increasing thickness indicates more difficulty in the exciton radiative recombination for thicker $ReSe_2$, which may be caused by limited amount of phonon. Thickness-dependent optical absorption spectra in the wavelength range of 400 nm–1045 nm are plotted in Fig. 1(f). The optical absorbance (Abs) is calculated from the following function:

$$\mathrm{Abs} = \log_{10} \frac{(I_0 - I_B) - (I_S - I_B)}{(I_0 - I_B)}, \tag{1}$$

where I_0 and I_S are the intensities of light transmitted through the fused quartz substrate and $ReSe_2$ flake, respectively. I_B denotes the background noise intensity from instruments and surrounding environment. As expected, the measured absorption spectra show that thicker flake retains much more absorption which is consistent with the AFM data. The absorption peak position changes from 410 nm to 420 nm as thickness increases. In addition, the absorption peak around 950 nm corresponds to the exciton resonant absorption as shown in Fig. 1(e).

In order to analyze the chemical composition, the scanning electron microscopy (SEM) and energy dispersive spectroscopy (EDS) are performed (Fig. S4). The results indicate the homogeneous distribution of Re and Se elements, and the atomic ratio of Re to Se is 1:1.18, implying the vacancy defect in the measured samples.

3. Experimental details

3.1. Sample fabrication and characterization

$ReSe_2$ flakes were mechanically exfoliated from the bulk $ReSe_2$ crystal via using a Stock tape to transfer it onto a fused SiO_2 substrate (1-mm thick). Atomic force microscopy (WITec Alpha 300) in tapping mode was used to determine the thicknesses of the measured areas (from 3.6 nm to 49.0 nm), with 0.6-nm vertical resolution and 8-nm resolution in transversal direction. Raman spectra and PL spectra were measured with 532-nm laser excitation in the WITec Alpha 300 at room temperature. The light source for absorption measurements was a halogen lamp. The transmitted light is captured with a microscope objective (100×, NA = 0.9) and directed to a spectrometer (PG 2000, Ideaoptics) equipped with a CCD camera (Exmor CMOS Sensor, Sony). MERLIN Compact (Zeiss) is used to perform scanning electron microscopy (SEM) and energy dispersive spectroscopy (EDS).

3.2. Transient reflection measurements

A Yb fiber-based laser (Menlo Systems) was used to provide ultrashort pulses with a central wavelength of 1040 nm and a 100-MHz repetition rate. The pulse width is $\sim$ 150 fs (FWHM). The majority of output was used as probe beam and a minority is separated to generate 520-nm pulse via second harmonic generation and used as pump pulse. The probe power was attenuated in a combination of half-wave plate and Glan–Taylor prism. Both pump pulses and probe pulses were focused onto the sample surface with a Gaussian spot, by using an objective lens (Tu Plan Flour 50×, NA = 0.8, Nikon). The transmitted beams were collected via another objective lens (Ph1 ADL 40×, NA = 0.55, Nikon). The transmitted pump beam was blocked with filters. This significantly improved the signal-to-noise ratio. The transmission change (ΔT) of probe beam due to the pump excitation was measured with a lock-in amplifier (SR865A, Stanford Research Systems) referenced to 1.5 kHz mechanically chopped pump light (SR542, Stanford Research Systems).

4. Results and discussion

To study carrier and exciton dynamics of $ReSe_2$ with different thicknesses, we use a home-build pump-probe system to perform time-resolved ΔT measurement (see Fig. S5 for details). The time-resolved ΔT traces are obtained by exciting the $ReSe_2$ with 520-nm (2.4 eV) femtosecond pulse and monitoring the transmittance change of 1040-nm (1.2 eV) probe pulses as a function of time delay between pump and probe pulses. The relaxation of equilibrium carriers in the energy band determines the time-evolution of ΔT signal. Figures 2(a)–2(f) show the time-resolved ΔT curves of six $ReSe_2$ flakes whose thicknesses are 3.6 nm, 7.2 nm, 10.2 nm, 14.9 nm, 18.6 nm, and 49.0 nm, respectively.

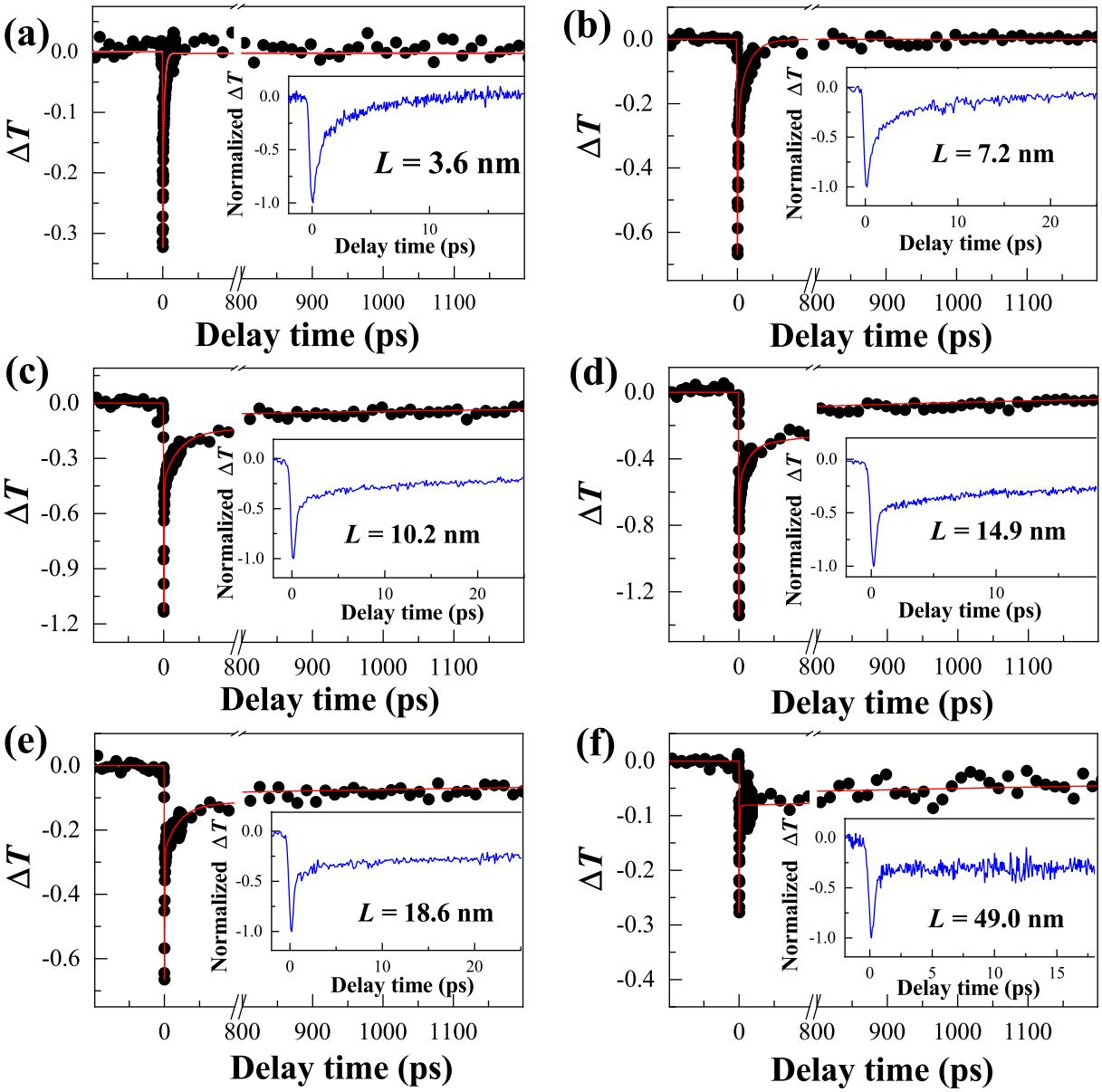


Fig. 2. (a)–(f) Time-resolved ΔT curves for $ReSe_2$ flakes of different thicknesses. The pump and probe powers are 60 μW and 40 μW, respectively. The polarization configuration was set parallel for pump and probe, and the pump polarization was along the *b* axis. The solid lines represent the fitting corresponding to a bi-exponential function.

After pump excitation, the ΔT signal increases within 0.9 ps which is limited by the resolution of our measurement system, and reaches a negative peak right (around zero-delay time). Then, the negative ΔT signal recovers slowly to zero. Negative ΔT signal indicates the photoinduced absorption (PA). The PA comes from the excited state absorption of nonequilibrium carriers since the photon energy of probe (1.2 eV) is smaller than the optical bandgap (> 1.29 eV) or the exciton energy state of all $ReSe_2$ samples.[19] Therefore, the intraband absorption of nonequilibrium carrier induces a negative ΔT signal. The resolution-limited enhancement of ΔT signal before 0 delay is caused by the carrier thermalization via carrier-carrier scattering and carrier-phonon scattering,[28] which rapidly expands the photoexcited carriers from the high-energy state toward the bottoms of energy bands, and establishing a quasi-equilibrium distribution for the formed hot carriers.[29] To analyze the subsequent relaxation process, the time-resolved curves are fit to a bi-exponential function as follows:

$$\Delta T = B\exp\left(\frac{-t}{\tau_1}\right) + C\exp\left(\frac{-t}{\tau_2}\right). \tag{2}$$

The fit parameters are denoted in B, C. Time-delayed t is the time interval between pump and probe pulses. τ_1 and τ_2 represent the fast decay time and the slow decay time, respectively. As shown in Figs. 2(a)–2(f), the experimental curves could be fit well by the bi-exponential decay function convoluted with a Gaussian response function.

Figure 3 shows the extracted time constants τ_1 and τ_2 for different thicknesses. Obviously, the fast relaxation times are in ps time scale in the measured six flakes. This lifetime

(τ_1), which is comparable to the lifetime of WS_2, should be attributed to the hot carrier relaxation and exciton formation by dissipating excess energy.[20,21,30–32] In this process, the decrease of signal is due to the fact that hot carriers could more efficiently induce the absorption coefficient change as compared with excitons. Thus, during the conversion of hot carriers to excitons, the ΔT signal decreases.

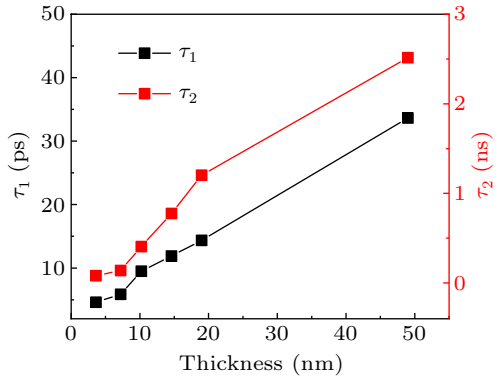


Fig. 3. Time constants extracted from bi-exponential fits as the function of film thickness.

Now let us explore the thickness-dependent exciton dynamics. The fast lifetime τ_1 monotonically increases from ~ 5 to ~ 34 ps as the $ReSe_2$ thickness increases (Fig. 3). Since the bandgap of $ReSe_2$ is nearly unchanged with thickness, the observed thickness dependence of lifetimes could not originate from band structure variation. It has been proved that hot carriers can couple to nearby traps or interfacial defects for relaxation in semiconductor quantum dots.[25,33] Based on this model, the defect plays an "elevator" role in assisting the electron transition from the high energy level to the low energy level, which provides an additional channel for cooling and accelerating intraband relaxation of carrier.[34] The defect density is enhanced at the surface and interfaces,[35] as a result, the defect density in few-layer $ReSe_2$ is larger than that of thicker flake, therefore the scattering probability caused by defects decreases with increasing the thickness of $ReSe_2$. As a result, the time constant (τ_1) increases as thickness of $ReSe_2$ increases.

The slow decay time, which corresponds to the recovery of negative ΔT signal to zero, reflects the bounded exciton recombination process between the energy states near the bottom of conduction band and the top of valence band in the indirect bandgap. Figure 3 shows that the decay time τ_2 has a similar trend to the fast time τ_1 as the $ReSe_2$ thickness increases. The τ_2 value increases from 81 ps for 3.6 nm to 2.5 ns for 49 nm. The thickness dependence of slow decay times τ_2 is mainly attributed to trap-mediated decay. Since defect densities of surface layers are much larger than that of other layers, the contribution of trap-mediated decay to thin layer is more efficient than that to thick layer. Our observation is consistent with the result of Wang *et al.* that τ_2 increases as the thickness increases.[36] Similar result has also been observed in ReS_2.[35]

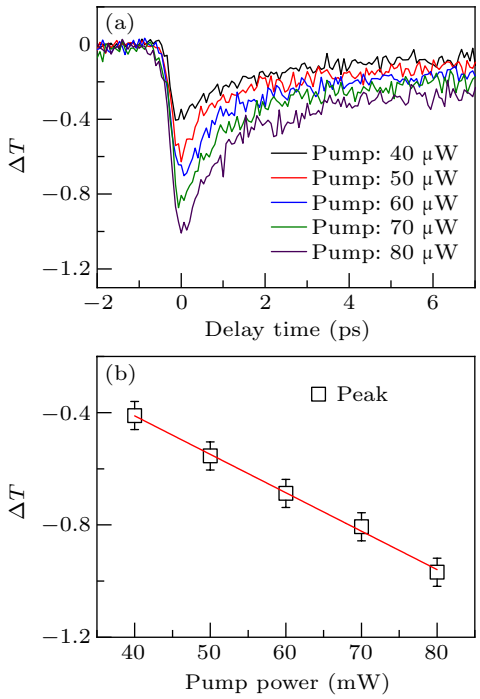


Fig. 4. (a) Time-resolved ΔT curves of 7.2 nm-thick $ReSe_2$ measured with different pump powers. (b) The peak value of ΔT (black squares) as a function of pump power. The red lines are linear fits.

To explore the influence of injected photocarrier densities, we measure the time-resolved ΔT traces of 7.2-nm-thick $ReSe_2$ flake with different pump power (Fig. 4(a)). It is found that the ΔT signal increases with pump power and the ΔT peak increases linearly with the pump power (Figs. 4(a) and 4(b)). Based on the thickness-dependent optical absorption spectra of $ReSe_2$ shown in Fig. 1(f), a peak carrier density n_0 injected by pump excitation is estimated from 1.4×10^{12} cm^{-2} for 7.2 nm (pump power 40 μW) to 8.7×10^{12} cm^{-2} for 49 nm (pump power 80 μW) at the center of the pump laser spot.[37] The Mott threshold ($\sim 10^{13}$ cm^{-2}) in typical 2D TMDs is higher than n_0.[38–40] This is confirmed by the linear dependence between pump power and the ΔT peak, as shown in Fig. 4(b). Generally speaking, slower decay dynamics with increasing pump power is typical hallmark of trapping-assisted recombination, because of the decrease of unoccupied defect states when the density of both injected carrier and defect state is comparable.[41–43] However, no pump power dependence of τ_2 is observed in the six measured flakes, which is supported by the normalized ΔT traces shown in Fig. S6. It shows that the n_0 is lower than the saturation density of defect state. Thus, the result indicates that defect state saturation hallmarks are absent in the six flakes. As the PL emission is very weak in these $ReSe_2$ flakes, the contribution of radiative channel is very limited. Moreover, nonradiative channel like phonon-involved scattering may also contribute to the exciton

recombination process, here the exciton recombination transfers its energy to the lattice. The observed τ_2 value for 7.2 nm has the same order of magnitude with the previous result that the lifetime of phonon-assisted recombination is $\sim$ 100 ps in ReS_2.[44] These pump power independent characteristics also rule out the EEA during the carrier relaxation process based on the following analysis: EEA is a typical Auger recombination process where a collision between two excitons causes one to recombine and the other to be excited to higher states.[41,45–52] The typical feature of EEA is that the fast component shows pump power dependent behavior and the lifetime of EEA also decreases when pump power increases since EEA enhances at high carrier density.[32,41]

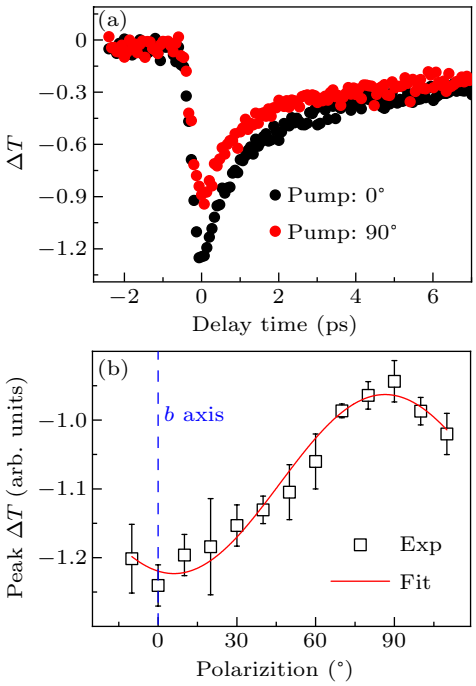


Fig. 5. (a) Time-resolved ΔT traces for the pump polarization along the 0° and 90° directions when the probe polarization is along 0°. (b) Peak ΔT signal as a function of pump polarization, red line is a cosine function fit.

Since $ReSe_2$ has a distorted 1T phase with triclinic symmetry of octahedral crystal structure, it is interesting to explore the effect of crystal symmetry on the ΔT signal. Figure 5(a) shows the dependence of ΔT curve on pump polarization for the 7.2-nm-thick $ReSe_2$ flake. The ΔT signal intensity changes with pump polarization while its decay time remains unchanged, which could be manifested by the independent normalized ΔT curves of pump polarization (Fig. S7(a)). It is obvious that the sample orientation does not affect the relaxation time. This polarization independence of decay times, which is consistent with former reports on monolayer, few-layer and bulk $ReSe_2$, implies that the behavior of excitonic dynamics is isotropic in the 2D plane.[19,21,22] Figure 5(b) depicts the peak ΔT value as a function of pump polarization. It is found that the peak ΔT value shows a two-fold symmetry and maximizes along b axis (*i.e.*, Re atom chains). As the pump polarization with an angle of θ with respect to b axis, the peak ΔT_θ value can be determined by the following functions:

$$\Delta T_\theta \propto \left(\frac{A_1 - A_2}{2}\right)\cos 2\theta + \left(\frac{A_1 + A_2}{2}\right), \tag{3}$$

$$\frac{\Delta T_{\max}}{\Delta T_{\min}} = \frac{A_1}{A_2}. \tag{4}$$

Here, A_1 (A_2) is absorption coefficient with respect to the polarization direction of incident light parallel (perpendicular) to b axis. $\Delta T_{\max}$ and $\Delta T_{\min}$ are the maximum and minimum of cosine function fit. The details of formula derivation are shown in Fig. S8. As the solid line shown, this pump polarization dependence of peak ΔT_θ can be well fitted with the cosine function. Based on Eq. (S7), the ratio of $\Delta T_{\max}/\Delta T_{\min} = 1.26 \pm 0.06$ can be obtained from the fit. According to the previous theoretical calculation[13] of optical absorption spectra of monolayer $ReSe_2$, we can get $A_1/A_2 \approx 1.25$ which is in accordance with the fitting result $\Delta T_{\max}/\Delta T_{\min} = 1.26 \pm 0.06$, supporting that the anisotropy of ΔT signal comes from the anisotropic optical absorption. To determine the origin of this polarization dependence, the optical absorption (calculated from $\alpha = -\log_{10}(T/T_{\text{sub}})$, where T and T_{sub} are the transmittances of the pump light through the sample and substrate, respectively) as a function of pump polarization was measured by blocking the probe beam in the pump–probe measurement (see Fig. S7(b) for details). The optical absorption is largest when the polarization of light is along with the b axis (*i.e.*, Re atom chains), which is consistent with the previous results[6] and the polarization dependence of peak ΔT. Therefore, the anisotropy of ΔT signal should come from the anisotropy of optical absorption. Similar to BP and SnSe, although the peak ΔT signal is dependent on polarization, its time evolution is independent of polarization.[53,54]

5. Summary

Time-resolved pump–probe transient transmission spectroscopy was employed to study the exciton dynamics of few-layer $ReSe_2$ prepared by mechanical exfoliation with a thickness ranging from 3.6 nm to 49.0 nm. The results reveal the pump-induced absorption of probe light at 1040 nm and thickness-dependent exciton dynamics. The fast relaxation time is attributed to the hot carrier relaxation and exciton formation and increases with thickness due to the decrease of scattering probability caused by defects. The slow relaxation time, corresponding to the exciton recombination is related to the trap-mediated exciton depopulation induced by defects, also get a larger contribution for thinner layers since the defect density of surface layers is larger than that of other layers. The linear pump power dependence of ΔT (peak) confirms that EEA are absent. The exciton dynamics is isotropic in the anisotropic 2D plane of $ReSe_2$. These findings imply

that the optical response process of $ReSe_2$ optoelectronic devices varies with the $ReSe_2$ thickness.

Acknowledgments

Project supported by the National Natural Science Foundation of China (Grant Nos. 12074202, 12174207, and 11974190) and the Natural Science Foundation of Tianjin City (Grant Nos. 20JCQNJC00020 and 22JCYBJC00390).

References

[1] Bae S and Sim S 2022 *J. Korean Phys. Soc.* **81** 532
[2] Zhang L, He D W, He J Q, Fu Y and Wang Y S 2019 *Chin. Phys. B* **28** 087201
[3] Ma J J, Wu K, Wang Z Y, Ma R S, Bao L H, Dai Q, Ren J D and Gao H J 2022 *Chin. Phys. B* **31** 088105
[4] Kumar N, He J, He D, Wang Y and Zhao H 2014 *Nanoscale* **6** 12690
[5] Wang P, Qu J, Wei Y, Shi H, Wang J, Sun X, Li W, Liu W and Gao B 2021 *ACS Appl. Mater. Interfaces* **13** 58144
[6] Ho C H, Lee H W and Wu C C 2004 *J. Phys.: Condens. Matter* **16** 5937
[7] Wolverson D, Crampin S, Kazemi A S, Ilie A and Bending S J 2014 *ACS Nano* **8** 11154
[8] Huang Y S, Ho C H, Liao P C and Tiong K K 1997 *J. Alloys Compd.* **262–263** 92
[9] Li K, Du C, Gao H, Yin T, Zheng L, Leng J and Wang W 2022 *ACS Appl. Mater. Interfaces* **14** 33589
[10] Alcock N and Kjekshus A 1965 *Acta Chem. Scand.* **19** 79
[11] Wen W, Zhu Y, Liu X, Hsu H P, Fei Z, Chen Y, Wang X, Zhang M, Lin K H, Huang F S, Wang Y P, Huang Y S, Ho C H, Tan P H, Jin C and Xie L 2017 *Small* **13** 1603788
[12] Ho C H, Huang Y S, Tiong K K and Liao P C 1998 *Phys. Rev. B* **58** 16130
[13] Zhang E, Wang P, Li Z, Wang H, Song C, Huang C, Chen Z G, Yang L, Zhang K, Lu S, Wang W, Liu S, Fang H, Zhou X, Yan H, Zou J, Wan X, Zhou P, Hu W and Xiu F 2016 *ACS Nano* **10** 8067
[14] Zhong H X, Gao S, Shi J J and Yang L 2015 *Phys. Rev. B* **92** 115438
[15] Arora A, Noky J, Drüppel M, Jariwala B, Deilmann T, Schneider R, Schmidt R, Del Pozo-Zamudio O, Stiehm T, Bhattacharya A, Krüger P, Michaelis de Vasconcellos S, Rohlfing M and Bratschitsch R 2017 *Nano Lett.* **17** 3202
[16] Zhao H, Wu J, Zhong H, Guo Q, Wang X, Xia F, Yang L, Tan P and Wang H 2015 *Nano Res.* **8** 3651
[17] Ho C H, Liao P C, Huang Y S, Yang T R and Tiong K K 1997 *J. Appl. Phys.* **81** 6380
[18] Jariwala B, Voiry D, Jindal A, Chalke B A, Bapat R, Thamizhavel A, Chhowalla M, Deshmukh M and Bhattacharya A 2016 *Chem. Mater.* **28** 3352
[19] Jiang S, Yang J, Shi Y, Zhao J, Xie C, Zhao L, Fu J, Yang P, Huan Y, Xie Q, Jiang H, Zhang Q, Wang X, Su F and Zhang Y 2020 *Nano Res.* **13** 667
[20] Yang J, Jiang S, Xie J, Jiang H, Xu S, Zhang K, Shi Y, Zhang Y, Zeng Z, Fang G, Wang T and Su F 2021 *ACS Nano* **15** 16760
[21] Liu F, Zhao X, Yan X Q, Xie J, Hui W, Xin X, Liu Z B and Tian J G 2019 *J. Appl. Phys.* **125** 173105
[22] He J, Zhang L, He D, Wang Y, He Z and Zhao H 2018 *Opt. Express* **26** 21501
[23] Zhang L, He D, He J, Fu Y, Bian A, Han X, Liu S, Wang Y and Zhao H 2019 *Opt. Express* **27** 17851
[24] Choi Y, Kim K, Lim S Y, Kim J, Park J M, Kim J H, Lee Z and Cheong H 2020 *Nanoscale Horizons* **5** 308
[25] Mak K F, Lee C, Hone J, Shan J and Heinz T F 2010 *Phys. Rev. Lett.* **105** 136805
[26] Liu D, Hong J, Wang X, Li X, Feng Q, Tan C, Zhai T, Ding F, Peng H and Xu H 2018 *Adv. Funct. Mater.* **28** 1804696
[27] Huang Y, Gu Y, Wu X, Ge R, Chang Y F, Wang X, Zhang J, Akinwande D and Lee J C 2021 *Front. Nanotechnol.* **3** 782836
[28] Li Y C, Ge C, Wang P, Liu S, Ma X R, Wang B, Song H Y and Liu S B 2022 *Chin. Phys. B* **31** 067102
[29] Jin T X, Yang J Y, Fang Y, Han Y b and Song Y L 2018 *Chin. Phys. B* **27** 054208
[30] Ceballos F, Cui Q, Bellus M Z and Zhao H 2016 *Nanoscale* **8** 11681
[31] He J, He D, Wang Y, Cui Q, Ceballos F and Zhao H 2015 *Nanoscale* **7** 9526
[32] Zhao S, He D, He J, Zhang X, Yi L, Wang Y and Zhao H 2018 *Nanoscale* **10** 9538
[33] Schroeter D F, Griffiths D J and Sercel P C 1996 *Phys. Rev. B* **54** 1486
[34] Shi H, Yan R, Bertolazzi S, Brivio J, Gao B, Kis A, Jena D, Xing H G and Huang L 2013 *ACS Nano* **7** 1072
[35] Sim S, Lee D, Lee J, Cha M, Cha S, Heo W, Cho S, Shim W, Lee K, Yoo J, Prasankumar R P, Choi H and Jo M H 2020 *Phys. Rev. B* **101** 174309
[36] Wang H, Zhang C and Rana F 2015 *Nano Lett.* **15** 8204
[37] Ceballos F and Zhao H 2017 *Adv. Funct. Mater.* **27** 1604509
[38] Chernikov A, van der Zande A M, Hill H M, Rigosi A F, Velauthapillai A, Hone J and Heinz T F 2015 *Phys. Rev. Lett.* **115** 126802
[39] Pogna E A A, Marsili M, De Fazio D, Dal Conte S, Manzoni C, Sangalli D, Yoon D, Lombardo A, Ferrari A C, Marini A, Cerullo G and Prezzi D 2016 *ACS Nano* **10** 1182
[40] Steinhoff A, Rösner M, Jahnke F, Wehling T O and Gies C 2014 *Nano Lett.* **14** 3743
[41] Sun D, Rao Y, Reider G A, Chen G, You Y, Brézin L, Harutyunyan A R and Heinz T F 2014 *Nano Lett.* **14** 5625
[42] Sim S, Park J, Koirala N, Lee S, Brahlek M, Moon J, Salehi M, Kim J, Cha S, Sung J H, Jo M H, Oh S and Choi H 2016 *ACS Photon.* **3** 1426
[43] Parkinson P, Joyce H J, Gao Q, Tan H H, Zhang X, Zou J, Jagadish C, Herz L M and Johnston M B 2009 *Nano Lett.* **9** 3349
[44] Wang X, Shinokita K, Lim H E, Mohamed N B, Miyauchi Y, Cuong N T, Okada S and Matsuda K 2019 *Adv. Funct. Mater.* **29** 1806169
[45] Kumar N, Cui Q, Ceballos F, He D, Wang Y and Zhao H 2014 *Phys. Rev. B* **89** 125427
[46] Yuan L and Huang L 2015 *Nanoscale* **7** 7402
[47] Yuan L, Wang T, Zhu T, Zhou M and Huang L 2017 *J. Phys. Chem. Lett.* **8** 3371
[48] Liu B, Meng Y, Ruan X, Wang F, Liu W, Song F, Wang X, Wu J, He L, Zhang R and Xu Y 2017 *Nanoscale* **9** 18546
[49] Yu Y, Yu Y, Xu C, Barrette A, Gundogdu K and Cao L 2016 *Phys. Rev. B* **93** 201111
[50] Cunningham P D, McCreary K M and Jonker B T 2016 *J. Phys. Chem. Lett.* **7** 5242
[51] Mouri S, Miyauchi Y, Toh M, Zhao W, Eda G and Matsuda K 2014 *Phys. Rev. B* **90** 155449
[52] Zhang T and Wang J 2021 *ACS Photon.* **8** 2770
[53] He J, He D, Wang Y, Cui Q, Bellus M Z, Chiu H Y and Zhao H 2015 *ACS Nano* **9** 6436
[54] Zhang C, Ouyang H, Miao R, Sui Y, Hao H, Tang Y, You J, Zheng X, Xu Z, Cheng X A and Jiang T 2019 *Adv. Opt. Mater.* **7** 1900631